Accepted Manuscript

Effect of vacuum annealing on structural, electrical and thermal properties of e-beam evaporated Bi2Te3 thin films

C. Sudarshan, S. Jayakumar, K. Vaideki, C. Sudakar

Please cite this article as: C. Sudarshan, S. Jayakumar, K. Vaideki, C. Sudakar , Effect of vacuum annealing on structural, electrical and thermal properties of e-beam evaporated Bi2Te3 thin films. The address for the corresponding author was captured as affiliation for all authors. Please check if appropriate. Tsf(2017), doi: 10.1016/j.tsf.2017.03.043

Effect of vacuum annealing on structural, electrical and thermal properties of e-beam evaporated Bi_2Te_3 thin films

C. Sudarshan,[a] S. Jayakumar,[b,*] K. Vaideki,[a] and C. Sudakar[c]

[a] Thin Film Centre, PSG College of Technology, Coimbatore 641004, India
[b] Department of Physics, PSG Institute of Technology and Applied Research, Coimbatore 641062, India
[c] Multifunctional Materials Laboratory, Department of Physics, Indian Institute of Technology Madras, Chennai 600036, India

*Corresponding author e-mail address: s_jayakumar_99@yahoo.com

Abstract:

Nanocrystalline thin films of a V-VI compound Bi_2Te_3 are fabricated with uniform thickness by e-beam evaporation at room temperature. The as-deposited films are stoichiometric, monophasic, highly strained and polycrystalline. We studied the effect of vacuum annealing (at a pressure of $\sim 3 \times 10^{-6}$ mbar) on composition, structure, optical and electrical properties of these films. It is observed that, as the annealing temperature increases (from 100 °C to 300 °C), the crystallites grow with a preferential orientation along (110) planes with slight increase in the crystallite size from ~14 nm to 30 nm. This is associated with the breaking of quintuple layers and rearrangement of crystallographic planes in the crystallites with Te rich surface emerging on vacuum annealing as evidenced from the XRD, Raman and high-resolution TEM studies. The direct bandgap (0.116 eV) of as-deposited Bi_2Te_3 changes from 0.092 eV to 0.113 eV on annealing at 100 °C to 300 °C, respectively. Interestingly, we observe a gradual change from a semiconductor to metallic behaviour on annealing the samples from 100 °C to 300 °C. Such a transition from negative temperature coefficient (NTC) to positive temperature coefficient (PTC) is seen mainly due to the percolation of Te - rich crystallite surfaces, which evolve as the annealing temperature increases. While the films annealed at 200 °C and 250 °C shows a broad semiconductor to metallic transition at ~ 150 K and 200 K respectively, the thin films annealed at 300 °C are found to exhibit complete metallic behavior below room temperature. The electrical property and Seebeck coefficient studies with power factors in the range of ~ 4 to 12 $\times 10^{-4}$ W/K^2m for film annealed above 200 °C suggest that the vacuum annealed Bi_2Te_3 thin films are favorable for thermoelectric applications.

1. Introduction

Bismuth Telluride (Bi_2Te_3) is a V-VI layered structure semiconductor with a rhombohedral unit cell (space group: $R\bar{3}m$) [1]. Bi_2Te_3 is highly anisotropic due to its layered structure and generally grows parallel to c-axis. Due to its narrow bandgap and unique thermoelectric characteristics at room temperature, Bi_2Te_3 is used in thermoelectric generators, thermo-coolers, and thermocouples [2-4]. It is also used as sensor and finds application in optoelectronics such as photoconductive targets for TV cameras and IR spectroscopy [5, 6].

In recent times, a tremendous improvement in the bulk Bi_2Te_3 properties and its applications to various fields have been discussed [7, 8]. However, in low dimensional structural forms the material properties differ and various studies are being carried out on this compound in thin films to improve their thermoelectric properties [9]. At small scale, i.e., in thin films and nanostructures, there exist a great challenge to stabilize the structure and stoichiometry of Bi_2Te_3. Thin film fabrication is the most suitable technique that will be useful in semiconductor industry for producing low-dimensional thermoelectric devices. One of the main challenges that remain to be addressed is to fabricate high-quality thin films with excellent thermoelectric performance. Bi_2Te_3 thin films have been fabricated by various deposition techniques such as co-evaporation [10-12], evaporation [13, 14], flash evaporation [15], co-sputtering [16], metal organic chemical vapour deposition (MOCVD) [17, 18], pulsed electrodeposition [19], ion beam sputtering [20] and electrodeposition [21]. Due to volatile nature of Te most of these studies report the post annealing effects on structure and optical properties of Bi_2Te_3 thin films. Electron beam (e-beam) evaporation is one other promising technique to fabricate Bi_2Te_3 thin films that has scarcely been explored. Bi_xTe_y-based alloy thin films [22], influence of doping on the structural and optical properties of Bi_2Te_3 [23], and thermoelectric properties of Sb_2Te_3 [24] are few of the reports that have used

the e-beam evaporation as the deposition technique. While there exist large volume of reports on the physical and thermoelectric properties of Bi_2Te_3 prepared by other techniques, more specifically by thermal evaporation, e-beam deposited thin films are scarce and would provide its own merits on properties of Bi_2Te_3 thin films. E-beam evaporation uses source to substrate distances more than 10 cm in comparison < 5 cm distance used in most of thermal evaporation and sputtering techniques. This avoids the unintentional substrate heating thereby minimizing the diffusion or evaporation of deposited atoms. In e-beam technique, bombarding the target material with an electron beam causes atoms from the source material to evaporate into the gaseous phase. These atoms solidify into a uniform thin coating on the substrate. The temperature of the substrate remains at ambient without significantly getting altered and the substrate surface damage is less due to impinging atoms, unlike in the sputtering that induces more damage because of the high-energy particles. Due to the high energy employed for the e-beam the source material is completely molten and made compositionally homogeneous before it vaporizes and gets deposited on to the substrate. The deposition rate in this process can be controlled to as low as 1 nm per minute to as high as few micrometers per minute. The material utilization efficiency is high relative to other methods and the process offers structural and morphological control of films.

In this paper we demonstrate that Bi_2Te_3 thin films can be deposited at room temperature with crystalline structure having near-stoichiometric composition by e-beam evaporation of bulk Bi_2Te_3 under optimized conditions. Further we have studied the post-annealing effect (under a pressure of $\sim 3 \times 10^{-6}$ mbar up to a temperature of 300 °C) on the structure, morphology, optical, and electrical properties of these films. We find that the crystallinity of the as-deposited Bi_2Te_3 improves with the annealing while the morphology and stoichiometry show slight changes. Interestingly, the temperature dependent resistivity measurements show that the as-deposited films are semiconductor-like with NTC response

and vacuum annealing transforms the film to metal-like with a PTC on annealing to more than 250 °C for 1 h. The samples annealed at 200 °C and 250 °C exhibit a broad hump in the resistivity *vs* temperature plots at ~ 150 K and ~200 K respectively, indicating a semiconductor to metallic transition in these Bi_2Te_3 films. Samples annealed at 300 °C are completely metallic in the resistivity *vs* temperature response. We also discuss the electrical properties and show that the power factor of the films annealed below 200 °C is between 1 to 3×10^{-4} W/K^{2}m, whereas the samples annealed at temperature above 200 °C exhibits an improved power factors in the range of ~ 4 to 12×10^{-4} W/K^{2}m estimated from the Seebeck coefficients measured with an applied temperature gradients of 30 °C to ~ 150 °C.

2. Experimental:

Bismuth telluride thin films were fabricated by electron beam evaporation technique using a HINDHI-VAC vacuum unit (model: 12A4D) fitted with electron beam power supply (model: EBG-PS-3K). High pure bismuth telluride (Alfa Aesar: 99.999%) chunks of few mm size, loaded in a graphite crucible and kept in water cooled copper hearth of the electron gun, is used as a source material. The Bi_2Te_3 chunks (~ 120 mg) were vapourised by means of an electron beam collimated from the DC heated tungsten filament cathode. The surfaces of the Bi_2Te_3 chunks were bombarded by 180° deflected e-beam at an accelerating voltage of 4.5 kV and with a power density of 1.5 kW/cm^2. The Bi_2Te_3 film was deposited at room temperature and base pressure of ~3 ×10^{-6} mbar on ultrasonically cleaned glass substrates kept at a distance of 12 cm from the crucible. The composition (Bi:Te ratio) and thickness of the deposited film depend on the power used for source and the distance between the source and the substrate. We have optimized both the power and the substrate position in the e-beam set up to obtain the Bi_2Te_3 thin films (see Table 1). In the e-beam setup the distance between the source and the center of the substrate holder is ~ 12 cm. While the substrate holder is quite large (~24 cm in dia.) and the substrates size we used are 7.5 cm × 1 cm. These substrates are

positioned at different distances radially from the center of the substrate holder along the vertical direction (Fig.1). The distance between the successive substrates are 3 cm apart and are marked as 1, 2, 3 and 4 in the schematic figure of the e-beam set up shown in the Fig.1. As can be seen from the Table 1, the near- stoichiometric composition of Bi_2Te_3 was obtained for the films deposited on substrate positioned at the centre of the substrate holder with a source power of 67.5 W (at a fixed voltage to the electron gun of 4.5 kV). The deposited films are found to be Bi rich and Te rich for the source power of 45 W and 90 W respectively. We also found that the films deposited become more of Te-rich when the substrates are positioned far from the center of the holder for a fixed source power. The near-stoichiometric thin film samples are deposited on the substrates positioned at the center of the holder using source power 67.5 W were studied in the present work. The thickness variation along the length (7.5 cm) of the substrate is found to be within 5 % variation. The as-deposited thin films of Bi_2Te_3 are referred to as BT-AD in the text. These as-deposited Bi_2Te_3 films were further post-annealed at 100, 150, 200, 250 and 300 °C for 60 minutes under vacuum at a pressure of ~ 3×10^{-6} mbar. After annealing, the samples were allowed to cool naturally to room temperature while maintaining the pressure at ~3×10^{-6} mbar. These samples are designated as BT-T (where 'T' is the vacuum annealing temperature).

The structural analysis of the samples were carried out by X'pert-pro PANalytical X-ray diffractometer operated at 30 kV with filtered Cu Kα_1 radiation of wavelength 1.5406 Å. The topographic details were collected using FEI Quanta FEG 200/FEG 400 Field Emission Scanning Electron Microscope (FESEM). The thickness of the e-beam deposited films was measured from the cross-sectional FESEM micrographs. Energy dispersive X-ray Spectroscopy (EDS) in the FESEM is used to estimate the composition of the films with an uncertainty of ~0.5 *at.*%. The microstructure and crystalline quality were also tested using JEOL JEM 2100 High Resolution Transmission Electron Microscope (HRTEM) operating at

200 kV. The surface topography of the films was examined by an atomic force microscopy (from NT-MDT, Russia) in a semi contact mode. The optical bandgap of the films were estimated by measuring diffuse reflection spectra (Perkin Elmer 2 plus) in the range of 500 to 4000 cm^{-1} at room temperature. The Hall coefficient was measured using a Hall measurement system from ECOPIA (HMS-3000 with B= 0.553 T) in the Van der Pauw configuration at room temperature. Low temperature resistivity measurements were carried out using a Keithley 2400 current source meter in a home-built four probe set up kept at a pressure of 10^{-2} mbar. The conductivity is measured with an uncertainty of *ca.* 5 % and the charge carrier mobility and concentration are measured with an uncertainty of *ca.* 10 %. Raman spectroscopic studies of Bi$_2$Te$_3$ thin film were carried out at room temperature using a Horiba Jobin-Yvon (HR800 UV) micro-Raman spectrometer with a 488 nm excitation line of Ar ion laser. Seebeck coefficient of thin films coated on 7.5 cm long and 1cm wide glass substrates were measured using a home-built set up. A temperature gradient of ~ 30 °C to ~165 °C was maintained between the hot and cold ends made of Cu block. The cold end was kept at 4 °C using a cold water circulation. The temperature of hot end was varied by a resistive heater using a temperature controller. The temperature gradient and Seebeck voltage were measured with good thermal and electrical contacts with in a distance of 5 cm. The Seebeck coefficient was obtained by taking the ratio of Seebeck voltage and temperature gradient with a measured uncertainty ~ 5 %. The thermoelectric power factor was calculated using the measured values of Seebeck coefficient and the electrical conductivity.

3. Results and discussion:

X-ray diffraction (XRD) patterns of as-deposited and post-annealed bismuth telluride films are shown in Fig. 2(a). The Bi$_2$Te$_3$ phase formation with a rhombohedral (space group $R\bar{3}m$) crystal structure in these films were confirmed by comparing the patterns with a standard Bi$_2$Te$_3$ file (ICDD # 015-0863). The XRD patterns are indexed using a hexagonal

(*hkl*) notation [25]. BT-AD film shows X-ray reflections at 2θ ~ 23.24°, 27.31°, 38.01° and 40.81° which correspond to (101), (015), (1010) and (110) planes, respectively. Relative intensities of X-ray reflections along with strong (015) peak revealed the similarity of BT-AD sample to a polycrystalline powder pattern (Fig.2a). Broad peaks from BT-AD films indicate the presence of nanocrystallites in this sample. On post-annealing treatment, the relative intensity of the diffraction peaks change and (110) slowly evolves to be the strongest reflection, indicating a change in the preferential orientation of crystallites with vacuum annealing. This reveals that the vacuum annealing promotes thin films to grow along (110) plane parallel to the surface with their *c*-plane oriented perpendicular to the plane of substrate. We also note that as these rearrangement of atomic planes take place, especially for the thin films annealed at 100 °C and 150 °C, a small fraction of Bi rich phase, most likely Bi_4Te_3 or Bi_7Te_3, segregates into a secondary phase with a broad low intense peak, before the crystallites finally get converted into a pure Bi_2Te_3 phase for annealing above 150 °C [26]. It should be noted that these secondary phases were not seen in the BT-AD films. Although a possible reason could be that the secondary phases might exist in amorphous form in BT-AD films, we believe the appearance of secondary phases could be due to the local variations in the composition due to vacuum annealing that sets up a small local inhomogeneity. The crystallographic planar rearrangements due to such variations can lead to the appearance of small fraction of secondary phases as found in BT-100 and BT-150 films. This is also consistent with the analyses from the Raman spectra discussed in the following section. Such phases disappear at high temperatures as the particle homogenize. Similar annealing dependent Bi-rich phase segregation has been reported earlier and is mainly attributed to the local disorder and compositional variations that arise due to the atomic rearrangements of crystallites [27, 28]. With increase in annealing temperature, an improved crystallinity is also revealed in the films.

The lattice parameters a and c were estimated from Reitveld refinement of XRD patterns using X'pert Highscore Plus software. Table 1 lists the estimated lattice parameters, for BT-T thin films from the best refinement fits obtained for Bi_2Te_3 phase along with the estimated particle size and microstrain. The changes in the lattice parameter a and c and c/a ratio as a function of annealing temperature is plotted in Fig. 2(b). The lattice parameters of BT-AD sample are $a = 4.3995$ Å and $c = 29.4640$ Å with c/a ratio 6.697. The lattice parameter a is found to be around 4.3995 Å for BT-AD films (Fig.2b) on vacuum annealing at 100 °C. The lattice parameter increases to 4.4225 Å before falling sharply down to 4.3766 Å for BT-150 films. On further annealing at higher temperature the lattice parameter a increases gradually to 4.3830 Å and become constant for T > 250 °C. The lattice parameter c shows continuous increase with the annealing temperature with $c = 29.4640$ Å for BT-AD to $c = 30.4255$ Å for BT-300 thin films (Fig.2b). It is observed that this c/a ratio increases from 6.697 Å to 6.937 Å as the annealing temperature increases to 300 °C regardless of the slight variations observed in a and c for each sample. BT-300 has unit cell constants $a = 4.3858$ Å and $c = 30.4255$ Å similar to the values of hexagonal unit cell in bulk Bi_2Te_3 [29]. These trends in the lattice parameter values suggest that the unit cell volume of Bi_2Te_3 increases during the annealing process. The smaller volume at low temperatures can be attributed to the compressive strain and atomic dislocations that may exist in the films. Strain can be induced in the Bi_2Te_3 films during the deposition process. Since the microstrain is the reason for the appearance of dislocation in the films, a decrease in the estimate of microstrain (Table 1) with vacuum annealing temperature indicates a decrease in the lattice imperfection and the formation of high quality films [30]. The trend in lattice parameter 'a' below T<150 °C is consistent with the change observed in microstrain suggesting the lattice parameter change are mostly influence by the residual microstrain in the crystallites. The films annealed above

250°C and 300°C are found to exhibit similar lattice constants, which indicate that the compressive strain in the Bi_2Te_3 films is almost relaxed at these annealing temperatures.

The average crystallite size is obtained from refined XRD data and Table 2 presents these data for the as-deposited and vacuum annealed samples. The crystallite size obtained from the Scherrer's equation $D = \frac{k\lambda}{\beta\cos\theta}$, [where β is the full width at half maximum (FWHM), λ is x-ray wavelength (Cu $K\alpha_1$, λ=1.5406Å) and k = 0.9 is a constant] for most intense peaks are also consistent with these average values. The crystallite size increases from ~13 nm for AD samples with the increase in annealing temperature and becomes almost constant beyond 250 °C (~ 30 nm). Upon reaching 300 °C, a significant re-crystallization takes place and the films are re-oriented in (110) direction.

Raman spectra can provide information on the structural changes that result due to annealing, including the appearance of impurity phase at the molecular level and surface phonon modes. The Raman spectra of BT-AD and BT-T thin films are shown in Fig. 3(a). For Bi_2Te_3 the layered rhombohedral structure with space group $R\bar{3}m$ contains five atoms in the primitive cell. This gives rise to 15 lattice vibrational modes at the Brillouin zone, which include three acoustic and 12 optical modes. The allowed modes in the irreducible representation for the bulk Bi_2Te_3 are $\Gamma_{bulk} = 2A_{1g} + 3A_{1u} + 2E_g + 3E_u$ [31, 32]. Due to inversion crystal symmetry, A_{1g} and E_g modes are Raman active, while A_{1u} and E_u modes are IR active. Three main peaks ~62 cm^{-1}, 102 cm^{-1}, and 137 cm^{-1} corresponding to A_{1g}^1, E_g^2 and A_{1g}^2 are generally reported for Bi_2Te_3 [33]. The Raman spectra of Bi_2Te_3 thin films in Fig. 3(b) show three main peaks ~ 98 – 100 cm^{-1}, 113 – 115 cm^{-1}, and 132 – 136 cm^{-1} corresponding to E_g^2, A_{1u} and A_{1g}^2 modes. A_{1g}^1 observed at ~ 62 cm^{-1} is not seen in our samples due to the weak resonant conditions of higher excitation photon energy and further, low intensity makes it difficult to resolve from the intense Rayleigh scattering. The stretching

mode A_{1g}^2 appears at ~ 132 cm^{-1} for BT-AD thin films which is red-shifted compared to the bulk Bi_2Te_3 values. Also the presence of A_{1g}^2 mode close to ~135 cm^{-1} suggest that the samples are characteristic of Te rich Bi_2X_3 (X = Te, Se).

It is also interesting to note that the intensity of A_{1g}^2 is higher than E_g^2 mode. The A_{1g} mode is due to the symmetric out-of-plane stretching of Te-Bi atoms vibrating in the opposite directions, whereas E_g mode is due to the symmetric in-plane bending and shearing of the upper two layers of Te-Bi atoms vibrating in the same direction [34]. The higher intensity of A_{1g} mode compared to the E_g mode, which is in contrary to the bulk spectra, indicate the samples are mostly oriented along the layered planes on the substrate. It is interesting to note that the A_{1g}^2 and E_g^2 modes get red-shifted on vacuum annealing (for T > 100 °C) of BT-AD. Also, the strong A_{1u} mode which is otherwise IR active in bulk Bi_2Te_3 became Raman active in Bi_2Te_3 thin films. A_{1u} mode is seen in the thin films because of the reduction or the breaking of the symmetry of Bi_2Te_3 films. Interestingly, in our study all the vacuum annealed films exhibit the strongest peak at ~115 cm^{-1}which is likely to originate from the Te rich surfaces of crystallites [35, 36]. Mislaid neighboring atoms and electron density at the surface are highly energetic and are more likely to move out of plane breaking the symmetry along c-axis [37]. These structural variations induced by the surface kinetics make the A_{1u} mode Raman active [38]. This A_{1u} mode composed of longitudinal optical phonons can be explained by surface phonon mode, which is only observed in nano-sized materials [39, 40].

In Fig. 3(c) the peak position of A_{1g}^2 and A_{1u} are plotted as function of annealing temperature. We can see that an obvious blue shift for A_{1g}^2 (132.4 to 136.2 cm^{-1}) and A_{1u} (113.6 to 115.5 cm^{-1}) modes for annealing temperatures up to 150°C, which indicates the atoms Bi and Te vibrate perpendicular to the layered surface. This could happen mainly due to smaller thickness of the films. At higher annealing temperatures, i.e $\geq$ 200°C there is red

shift in A_{1g}^2 (from 136.2 to 134.3 cm^{-1}) and A_{1u} (from 115.5 to 113.6 cm^{-1}) modes and these peak positions remain same for the samples annealed up to 300 °C. The occurrence of blue and red shift in Raman spectra has been reported in Bi_2Te_3 nanostructures exhibiting quantum confinement effect and in thin films where a reduction in the interlayer interaction was noted [41]. The frequency of in-plane vibration mode E_g^2= 100.58 cm^{-1}, in contrast, is very close to that from the bulk value 101.7 cm^{-1} [38, 42] for BT-AD film. With the vacuum annealing the peak position is seen to decrease. Further, the inhomogeneous broadening of E_g^2 mode shows there is strong electron-phonon interaction that could be linked to the strong interaction between the Bi_2Te_3 nanoparticle and the substrate. This indicates the presence of large strain in the as-deposited film compared to the vacuum annealed films.

From Table 3, another interesting observation is with respect to the calculated intensity ratio of $I(A_{1g}^2)/I(E_g^2)$ and $I(A_{1u})/I(E_g^2)$. These intensity ratios can be used to determine the number of quintuples in Bi_2Te_3 films [43]. A higher intensity ratio indicates high number density of quintuples and *vice versa*. For BT-100 samples this ratio is very high indicating slightest annealing of BT-AD films brings in a high density of quintuples. The decreasing intensity ratio of $I(A_{1g}^2)/I(E_g^2)$ and $I(A_{1u})/I(E_g^2)$ at high annealing temperature (>100 °C) under vacuum indicates that there is breaking of quintuples in the film [43]. This observation along with (110) oriented growths at high temperature annealing strongly suggest that vacuum annealing leads to breaking of quintuple layers with (110) oriented crystallites growth. The strongest A_{1u} mode seen in all the vacuum annealed thin films, which is likely to originate from Te rich crystallites suggest that crystallographic rearrangement of the planes most likely give rise to all the observations in XRD and Raman studies. Also the $I(A_{1u})/I(E_g^2)$ ratio is higher than $I(A_{1g}^2)/I(E_g^2)$ ratio. This indicates that the longitudinal optical phonon vibrations dominate compared to the out of plane vibrational modes. Thus,

from Raman spectra studies we conclude that, while the as-deposited and annealed films are crystalline, surface charges could construct stronger effect on these films [43].

Fig. 4 shows the topographic features of thin film surfaces as obtained from the FESEM images. The as-deposited sample show uniform thick films with smooth surfaces. The thickness of the films is found to be around 275 to 300 nm. This shows that the annealing process does not alter the thickness of the films significantly. The surface is comprised of nanocrystalline features, which in some regions seem to agglomerate. Thus the as-deposited sample grows in an island-growth mode forming the Bi_2Te_3 compound [44]. With annealing process there are minimal changes in the topographic features. It is considered that the annealing process contributes to the diffusion and agglomeration of the atoms. By comparing the surface images of as-deposited and annealed samples as shown in Fig 4(a-f), we could conclude that better crystallization is obtained after the vacuum annealing process which is consistent with the XRD patterns shown in Fig.2a. The grain size of annealed film is slightly bigger than as-deposited film. With increasing annealing temperature, more prominently at 250 °C and 300 °C, the grain boundary becomes poorly defined which indicate a possible surface reconstruction. This is consistent with the (110) getting stronger over the (015) reflections in XRD. Table 4 lists the thickness of the BT-AD and BT-T samples as estimated from the SEM images. Low magnification SEM images confirm a homogeneous deposition of nanocrystallite morphology and increased crystallite size with temperature. The composition of the films were found to be close to the expected 40:60 ratio for Bi:Te from the EDS spectra.

Fig. 5 shows the atomic force microscopic images of Bi_2Te_3 thin film surfaces. The surface topographic images in Fig. 5a to 5f illustrate the evolution of surface features and the changes in the surface roughness on vacuum annealing. The average and RMS roughness values are listed in Table 4 for all the samples. The BT-AD samples show larger boulder-like

vertically standing islands of grain with sizes ~200 to 400 nm. However, these grain-islands themselves are comprised of smaller features of few tens of nanometer. The oriented growth, more along the *c*-axis, observed from the XRD clearly indicate that these Bi_2Te_3 grains have grown as lumps of vertically standing particles. On annealing these nanometer scale features, within the islands grains smoothen out. The roughness of these samples were seem to remain ~ 9.5 to 10.5 nm for films annealed up to 200 °C. Slight decrease in the roughness with the annealing can be attributed to an increase in grain density causing uniform distribution on the film surface. The roughness for BT-250 films shows a slight increase due to the structural rearrangements of the grains. However, the roughness decreases in the case of BT-300 with more smooth surfaces of the island-grain features. The main changes observed in the surface topographic features could arise due to the suppression of crystal defects, pinholes, and micro-strain relaxation thus enhancing uniform and densely packed grains with *ab* planes growing parallel to the plane of the substrate.

The microstructure of Bi_2Te_3 samples was examined by HRTEM to determine the particle size and phase distribution (Fig. 6 and Fig. 7). The TEM samples were prepared by scraping off the films from the glass substrate and these fine particles were mounted on the carbon coated Cu grids. The bright field TEM images of BT-T films are shown in Fig. 6 (top panels) and the corresponding SAED patterns are given in the bottom panels. The BT-AD films are dense with particles in the size range of few tens of nanometer. The SAED patterns show dotted rings indicating the polycrystalline nature of the particles. The simulated patterns corresponding to the Bi_2Te_3 structure were overlaid on the experimental SAED data, which show the intensity of the (hkl) peak and their position in the SAED pattern. All the rings exactly match with the position of (hkl) peaks indicating the phase purity of the Bi_2Te_3 with no other secondary phases coexisting. Interestingly the SAED pattern of BT-AD sample shows some sort of oriented nature of the particles, which can be clearly discerned from the

non-uniform intensity distribution in the rings with existence of bright spots in the (015) peaks. With the annealing temperature the crystallites show slight increase in the size, however, without any change in the phase or decomposition of Bi_2Te_3. Representative SAED patterns shown from selected regions confirm the fact that the phase remains same on vacuum annealing. High-resolution TEM images were acquired from thin regions of the samples. The interior of crystallites are highly crystalline and in most of the HRTEM images the crystallites show lattice fringe width ~ 0.32 nm which correspond to the *d*-spacing of intense (015) reflection in Bi_2Te_3 structure. However, in many crystallites we observe distortions in the lattice images arising due to the presence of strain in the crystallites. With vacuum annealing the crystallite sizes do not change drastically. From the HRTEM of BT-300, we encountered crystallites with lattice fringes ~ 1 nm corresponding to the (003) planes. The TEM microstructural studies along with the EDS spectra acquired from these regions suggest the presence of stoichiometric crystallites at all the annealing temperatures.

Figure 8 shows the diffuse reflection spectra of as-deposited and post-annealed Bi_2Te_3 films. Change in the reflectance varies for the annealed films due to the variation of grain size and concentration of surface charge carriers. In both as-deposited and annealed samples, a considerable reduction in reflectance is seen around the absorption edge i.e. ~ 1220 cm^{-1}. Since Bi_2Te_3 exhibits double valence bands and double conduction bands it has both direct and indirect band gaps with energy values~ 0.13 eV and ~ 0.21 eV respectively [45, 46]. Both the direct and indirect band gap were calculated using Tauc equation $(\alpha h\nu)^n \propto (h\nu - E_g)$ with n=2 for direct bandgap and n=1/2 for indirect bandgap (Fig.8b and 8c). The DRS data collected with respect to a standard Ag film are converted into the Kubelka-Munk function F(R). Absorption coefficient α is equated to Kubelka-Munk function F(R), and plots of $[F(R)h\nu]^2 \propto (h\nu - E_g)$ and $[F(R)h\nu]^{1/2} \propto (h\nu - E_g)$ are made (Fig. 7b and 7c). The direct bandgap shows a linear increase in E_g from 0.092 eV for BT-100 to 0.113 eV for BT-300

except for an initial decrease found for BT-100 from 0.116 eV of BT-AD. With increase in the annealing temperature the decrease in the bandgap of the samples is consistent with the systematic changes observed in the lattice parameters from XRD. The band gap of BT-AD sample is found to be high with E_g= 0.116 eV. This trend in bandgap variation suggests that structural changes, decreasing microstrain and dislocation densities on vacuum annealing could possibly influence the band structure more than the minute differences in the composition. The bandgap values (E_g = 0.11 eV) of (110) plane dominated annealed films BT-250 and BT-300 is found to be close to the theoretical values given by Mishra *et al.* [47, 48] for perfect bulk like crystal. For as-deposited film, BT-AD, the larger bandgap compared to the low temperature annealed samples could be due to structural differences with large microstrain and dislocation density. Interestingly the indirect bandgap values estimated for these samples show lower values (~0.03 to 0.06 eV) than that reported in the literature [49].

The carrier concentration and carrier mobility of as-deposited and vacuum annealed samples at room temperature are shown in Fig. 9. All the films show negative value of Hall coefficient confirming the n-type characteristics of the films. With annealing temperature, the carrier concentration and mobility does not show significant changes and remain approximately at 4×10^{20} cm^{-3} and 10 cm^2/Vs respectively. Slight changes in these values could be due to the changes that occur in the crystallinity and surface defects of the films during vacuum annealing process. The variation of carrier mobility with annealing temperature shows opposite trend with respect to carrier concentration [50]. The decrease in carrier mobility with annealing temperature up to 150 °C may be attributed to the changes in microstructure. The grain size enlargement and aggregation lead to enhanced mobility.

Figure 10 shows the temperature dependent resistivity of Bi_2Te_3 thin films measured in the temperature range from 100K to 300 K. BT-AD, BT-100, and BT-150 samples show typical semiconducting behavior exhibiting a negative temperature coefficient. The resistivity

is found to differ slightly between these samples. Also the change in the resistance by lowering the temperature from 300 to 100 K is in the order of 10^{-1} to 10^{-2} Ωcm. Such a semiconducting behavior could be due to electron scattering between interlayer interactions of quintuples in the film. More interestingly we observe the change in the semiconductor behavior (i.e. negative temperature coefficient) of the Bi_2Te_3 films to metallic behavior (i.e. positive temperature coefficient) as seen from the resistivity *vs* temperature plots for high temperature (> 150 °C) annealed samples. BT-AD, BT-100 and BT-150 show NTC behavior, while BT-300 shows PTC behavior. A clear transition from the NTC to PTC behavior is seen in BT-200 and BT-250 samples in the resistivity *vs* temperature plots. With vacuum annealing there is an indication of quintuple breaking as discerned from Raman spectral studies. This could result in a slight increase of the resistivity as found in BT-100 and BT-150. For BT-200, BT-250, and BT-300, breaking of crystal symmetry along *c*-axis is discerned from the structural studies. For vacuum annealing temperatures > 150 °C thin films were found to exhibit a stronger (110) diffraction peak in its XRD pattern. Due to this the electron scattering gets reduced significantly. Such breaking of the crystal units can also lead to regions with Te-rich surfaces. As a result, metallic behavior begins to show up for the annealing temperatures ≥200 °C. BT-200 film exhibits an insulator characteristic from room temperature to 150 K and changes to metallic characteristics below 150 K. For BT-250 thin films this semiconductor to metallic transition is seen around 300 K. For BT-300, the resistivity *vs* temperature trend is completely metallic below 300 K. Such metallic behavior observed by Z. Yu *et.al.* [40] has been attributed to the decreased electron scattering due to broken crystal symmetry along the c-axis. The metallic conductivity is also shown in chlorine doped Bi_2Te_3 single crystals with the metallic characteristics mainly arising due to the charge transport in the layer planes through impurity band [51]. This clearly shows that the breaking of quintuples and growth along (110) planes with percolation of Te-rich surface of the

crystallites could give rise to the metallic behavior observed in the high temperature vacuum annealed samples.

We estimated the activation energy for the semiconducting region using the logarithmic variation of conductivity with inverse temperature (1/T) for the BT-T samples. The semiconductor regime shows two activation energies (E_a) in the temperature regions of 180-150 K and 150-300 K. The values of E_a has been calculated from the relation $\ln(\sigma) = \ln(\sigma_0) - E_a/k_B T$, where σ_0 [S.cm^{-1}] is the temperature independent conductivity, E_a is the activation energy in J, k_B is the Boltzmann constant, and T [K] is the absolute temperature. With the annealing temperature the activation energy decreases from 0.08 eV to 0.01 eV which attributes the changes of the crystallite size in the polycrystalline films. The decrease in the E_a is mainly due to changes in strain and dislocation density, and crystallographically reoriented crystallites with annealing temperature. The (015) oriented BT-AD films become (110) orientation-dominated films above 150 °C. Since the size of the crystallite differs only by 5 to 10 nm and the films were found to be near-stoichiometric at all the annealing temperatures, these factors may not influence the activation energy largely. Due to smaller size of the crystallites (10 to 30 nm) the grain boundary consists of defective atomic layers with significant distortion (see HRTEM images in Fig. 7b). These distorted grain boundaries scatter electron and impose the requirement of large energies for the electron to transport. Thus energy barrier can be directly correlated to the grain boundaries due to the accumulation of charges as proposed by Slater [52]. While we see the activation energy decreases with increasing annealing temperature with a sharp decrease at 100 °C, the semiconducting behavior switches to metallic as the Te rich grain boundaries mainly due to the reorientation of crystallites with preferential orientation along (110) grows at higher annealing temperature (> 200 °C) [53].

Figure 11(a) shows the result of room temperature measurement of Seebeck coefficient, resistivity and power factor of as deposited and annealed Bi_2Te_3 thin films. All the samples have negative value of Seebeck coefficients, which indicates that the films are n-type. The Seebeck coefficient increases from ~19 $\mu V/K$ for the as deposited film to a maximum of ~ 27 $\mu V/K$ for the film annealed at 250 °C. The power factor calculated from the electrical resistivity and Seebeck coefficient using the relation S^2/ρ. For T < 150 °C the power factor is ~ 2×10^{-4} W/K^2m. The power factor Bi_2Te_3 films is found to improve with a value 4 to 5×10^{-4} W/K^2m for samples annealed at >200 °C. This value is consistent with the reported power factor values of 4×10^{-4} W/K^2m prepared by RF magnetron method [54]. However it is lower than the value (9×10^{-4} W/K^2m) reported by Kim $et.$ $al.$[55], where the films are prepared by co-sputtering process. In general, the thermoelectric studies on most of the Bi_2Te_3 thin films reported the power factors in range between 2 to 9×10^{-4} W/K^2m [11, 12, 16, 20, 53, 55-59] with some of the reports giving values up to 20×10^{-4} W/K^2m [11, 12, 60, 61]. With the post annealing process the power factor is found to increase a bit. Very few paper have reported the values over 20×10^{-4} W/K^2m for the films deposited at high temperature [62]. In one of the studies the power factor of 80×10^{-4} W/K^2m was reported [63] which is exceptionally high compared to many of the reports with no explanation for such high values.

We carried out power factor estimation by finding the Seebeck coefficient with high temperature gradients (ΔT), i.e. by applying high temperatures to the hot end with respect to the fixed temperature (4 °C) of the cold end. The power factor increases two to three times as the ΔT is increased from 30 °C to ~165 °C (Fig. 11b) consistent with other reports. A maximum power factor of~ 12×10^{-4} W/K^2m is observed in BT-250 sample. For the samples where secondary phases were observed the power factor remains low even when measured at

high ΔT. The lower power factor of high temperature annealed Bi_2Te_3 (BT-300) compared to BT-200 and BT-250 suggests that an optimal vacuum annealing (~ 200 to 250 °C) provide right combination of microstructural, compositional and electrical properties yielding the larger power factor for e-beam evaporated thin films. Overall the power factor seem to strongly depend on the thin film processing conditions and therefore on the growth mechanism of Bi_2Te_3 crystallites. These results signify the fact that the microstructural changes upon annealing at elevated temperatures influence the electrical and thermoelectric properties of films with an improved Seebeck coefficient values for Bi_2Te_3 films annealed at above 200 and 250°C.

4. Conclusion:

In conclusion, we have fabricated nanocrystalline stoichiometric thin films of Bi_2Te_3 at room temperature using e-beam evaporation technique. The films are polycrystalline and exhibit semiconductor behavior. We studied the vacuum annealing effects on these as-deposited Bi_2Te_3films. The resistivity increases initially due to the crystallite growth and decreases for T > 150 °C, where crystallization with reorientation of crystallites preferably along (110) planes has been evidenced, which minimize the grain boundary scattering. The films annealed at < 150 °C exhibit a NTC behavior, while a clear transition from the NTC to PTC behavior is seen for samples annealed at 200 and 250 °C as evidenced in the resistivity *vs* temperature plots. At high temperatures of annealing (> 200 °C) a semiconductor to metal transition is seen to evolve and the films annealed at 300 °C completely show the metallic behavior. Such a metal-like behavior in the resistivity *vs* temperature plots can be attributed to the break in the crystal structures of quintuple layers, which lead to Te rich crystallite surfaces. Further electrical property studies suggest that the samples annealed at a temperature of 200 to 250 °C exhibit high power factors (~ 4 to 12 x 10^{-4} W/K^{2}m) and are favorable for thermoelectric applications.

References:

[1] D.M. Rowe, C.M. Bhandari, Modern thermoelectrics, Reston Pub. Co., Reston, Va., 1983.

[2] M.-Y. Kim, T.-S. Oh, Thermoelectric Characteristics of the Thermopile Sensors with Variations of the Width and the Thickness of the Electrodeposited Bismuth-Telluride and Antimony-Telluride Thin Films, Materials Transactions, 51 (2010) 1909-1913.

[3] M.-Y. Kim, T.-S. Oh, Thermoelectric Thin Film Device of Cross-Plane Configuration Processed by Electrodeposition and Flip-Chip Bonding, Materials Transactions, 53 (2012) 2160-2165.

[4] S. Herwaarden, Proc. 16th Int. Conf. on Thermoelectrics, DOI ((International Society of Thermoelectrics, 1997)) pp.47-55.

[5] D. Arivuoli, F.D. Gnanam, P. Ramasamy, Growth and microhardness studies of chalcogneides of arsenic, antimony and bismuth, Journal of Materials Science Letters, 7 (1988) 711-713.

[6] M. Stölzer, M. Stordeur, H. Sobotta, V. Riede, IR Transmission Investigations of $(Bi_{1-x}Sb_x)_2Te_3$ Single Crystals, physica status solidi (b), 138 (1986) 259-266.

[7] S.B. Riffat, X. Ma, Thermoelectrics: a review of present and potential applications, Applied Thermal Engineering, 23 (2003) 913-935.

[8] G. Chen, M.S. Dresselhaus, G. Dresselhaus, J.P. Fleurial, T. Caillat, Recent developments in thermoelectric materials, International Materials Reviews, 48 (2003) 45-66.

[9] R. Venkatasubramanian, E. Siivola, T. Colpitts, B. O'Quinn, Thin-film thermoelectric devices with high room-temperature figures of merit, Nature, 413 (2001) 597-602.

[10] J. George, B. Pradeep, Preparation and properties of co-evaporated bismuth telluride $[Bi_2Te_3]$ thin films, Solid State Communications, 56 (1985) 117-120.

[11] H. Zou, D.M. Rowe, G. Min, Growth of p- and n-type bismuth telluride thin films by co-evaporation, Journal of Crystal Growth, 222 (2001) 82-87.

[12] J.-H. Kim, J.-Y. Choi, J.-M. Bae, M.-Y. Kim, T.-S. Oh, Thermoelectric Characteristics of n-Type Bi_2Te_3 and p-Type Sb_2Te_3 Thin Films Prepared by Co-Evaporation and Annealing for Thermopile Sensor Applications, Materials Transactions, 54 (2013) 618-625.

[13] J. Dheepa, R. Sathyamoorthy, A. Subbarayan, Optical properties of thermally evaporated Bi_2Te_3 thin films, Journal of Crystal Growth, 274 (2005) 100-105.

[14] H.E.A. El-Sayed, Structural and optical properties of thermally evaporated Bi_2Te_3 films, Applied Surface Science, 250 (2005) 70-78.

[15] J. Dheepa, R. Sathyamoorthy, S. Velumani, Characterization of Bismuth Telluride thin films — Flash evaporation method, Materials Characterization, 58 (2007) 782-785.

[16] D.-H. Kim, E. Byon, G.-H. Lee, S. Cho, Effect of deposition temperature on the structural and thermoelectric properties of bismuth telluride thin films grown by co-sputtering, Thin Solid Films, 510 (2006) 148-153.

[17] A. Giani, A. Boulouz, F. Pascal-Delannoy, A. Foucaran, E. Charles, A. Boyer, Growth of Bi_2Te_3 and Sb_2Te_3 thin films by MOCVD, Materials Science and Engineering: B, 64 (1999) 19-24.

[18] A. Boulouz, S. Chakraborty, A. Giani, F.P. Delannoy, A. Boyer, J. Schumann, Transport properties of V–VI semiconducting thermoelectric BiSbTe alloy thin films and their application to micromodule Peltier devices, Journal of Applied Physics, 89 (2001) 5009-5014.

[19] V. Richoux, S. Diliberto, C. Boulanger, J.M. Lecuire, Pulsed electrodeposition of bismuth telluride films: Influence of pulse parameters over nucleation and morphology, Electrochimica Acta, 52 (2007) 3053-3060.

[20] Z.-h. Zheng, P. Fan, G.-x. Liang, D.-p. Zhang, X.-m. Cai, T.-b. Chen, Annealing temperature influence on electrical properties of ion beam sputtered Bi_2Te_3 thin films, Journal of Physics and Chemistry of Solids, 71 (2010) 1713-1716.

[21] R. Rostek, V. Sklyarenko, P. Woias, Influence of vapor annealing on the thermoelectric properties of electrodeposited Bi_2Te_3, Journal of Materials Research, 26 (2011) 1785-1790.

[22] T. Ino, S. Yamaguchi, Infrared and Thermoelectric Properties of Bi_xTe_y-Based Alloyed Thin Films, Sensors and Materials, 20 (2008) 447-455.

[23] B. Jariwala, D. Shah, N.M. Ravindra, Influence of doping on structural and optical properties of Bi_2Te_3 thin films, Thin Solid Films, 589 (2015) 396-402.

[24] H. Chang, M.-J. Kao, C.-H. Peng, C.-G. Kuo, K.-D. Huang, Thermoelectric Properties of Sb_2Te_3 Thin Films by Electron Beam Evaporation, Journal of Nanoscience and Nanotechnology, 11 (2011) 7491-7494.

[25] H.H. Soonpaa, Correlation of unit cell angle with transport properties in Bi_2Te_3, Journal of Physics and Chemistry of Solids, 25 (1964) 1107-1112.

[26] J.W.G. Bos, H.W. Zandbergen, M.H. Lee, N.P. Ong, R.J. Cava, Structures and thermoelectric properties of the infinitely adaptive series $(Bi_2)_m(Bi_2 Te_3)_n$, Physical Review B, 75 (2007) 195203.

[27] M. Winkler, X. Liu, J. König, S. Buller, U. Schürmann, L. Kienle, W. Bensch, H. Böttner, Electrical and structural properties of Bi_2Te_3 and Sb_2Te_3 thin films grown by the nanoalloying method with different deposition patterns and compositions, Journal of Materials Chemistry, 22 (2012) 11323-11334.

[28] Z. Aabdin, N. Peranio, M. Winkler, D. Bessas, J. König, R.P. Hermann, H. Böttner, O. Eibl, Sb_2Te_3 and Bi_2Te_3 Thin Films Grownby Room-Temperature MBE, Journal of Electronic Materials, 41 (2012) 1493-1497.

[29] J.R. Wiese, L. Muldawer, Lattice constants of Bi_2Te_3-Bi_2Se_3 solid solution alloys, Journal of Physics and Chemistry of Solids, 15 (1960) 13-16.

[30] D.V.S. B.S. Jariwala, Vipul Kheraj Substrate Temperature Effect on Structural Properties of Bi_2Te_3 Thin Films J. Nano- Electron. Phys., 3 (2010) 101-105.

[31] W. Kullmann, G. Eichhorn, H. Rauh, R. Geick, G. Eckold, U. Steigenberger, Lattice Dynamics and Phonon Dispersion in the Narrow Gap Semiconductor Bi_2Te_3 with Sandwich Structure, physica status solidi (b), 162 (1990) 125-140.

[32] Y. Zhao, X. Luo, J. Zhang, J. Wu, X. Bai, M. Wang, J. Jia, H. Peng, Z. Liu, S.Y. Quek, Q. Xiong, Interlayer vibrational modes in few-quintuple-layer Bi_2Te_3 and Bi_2Se_3 two-dimensional crystals: Raman spectroscopy and first-principles studies, Physical Review B, 90 (2014) 245428.

[33] W. Richter, C.R. Becker, A Raman and far-infrared investigation of phonons in the rhombohedral V_2–VI_3 compounds Bi_2Te_3, Bi_2Se_3, Sb_2Te_3 and $Bi_2(Te_{1-x}Se_x)_3$ ($0 < x < 1$), $(Bi_{1-y}Sb_y)_2Te_3$ ($0 < y < 1$), physica status solidi (b), 84 (1977) 619-628.

[34] J. Yuan, M. Zhao, W. Yu, Y. Lu, C. Chen, M. Xu, S. Li, K. Loh, QiaoliangBao, Raman Spectroscopy of Two-Dimensional $Bi_2Te_xSe_{3-x}$ Platelets Produced by Solvothermal Method, Materials, 8 (2015) 5007.

[35] A.S. Pine, G. Dresselhaus, Raman Spectra and Lattice Dynamics of Tellurium, Physical Review B, 4 (1971) 356-371.

[36] Q. Zhang, J. Zhang, M.I.B. Utama, B. Peng, M. de la Mata, J. Arbiol, Q. Xiong, Exciton-phonon coupling in individual ZnTe nanorods studied by resonant Raman spectroscopy, Physical Review B, 85 (2012) 085418.

[37] Y. Liang, W. Wang, B. Zeng, G. Zhang, J. Huang, J. Li, T. Li, Y. Song, X. Zhang, Raman scattering investigation of Bi2Te3 hexagonal nanoplates prepared by a

solvothermal process in the absence of NaOH, Journal of Alloys and Compounds, 509 (2011) 5147-5151.

[38] K.M.F. Shahil, M.Z. Hossain, D. Teweldebrhan, A.A. Balandin, Crystal symmetry breaking in few-quintuple Bi_2Te_3 films: Applications in nanometrology of topological insulators, Applied Physics Letters, 96 (2010) 153103.

[39] C. Wang, X. Zhu, L. Nilsson, J. Wen, G. Wang, X. Shan, Q. Zhang, S. Zhang, J. Jia, Q. Xue, In situ Raman spectroscopy of topological insulator Bi_2Te_3 films with varying thickness, Nano Research, 6 (2013) 688-692.

[40] Z. Yu, X. Wang, Y. Du, S. Aminorroaya-Yamni, C. Zhang, K. Chuang, S. Li, Fabrication and characterization of textured Bi_2Te_3 thermoelectric thin films prepared on glass substrates at room temperature using pulsed laser deposition, Journal of Crystal Growth, 362 (2013) 247-251.

[41] H. Rui, W. Zhenhua, L.J.Q. Richard, D. Conor, B. Ben, T.E. Kidd, C.C. Chancey, P.A.G. Xuan, Observation of infrared-active modes in Raman scattering from topological insulator nanoplates, Nanotechnology, 23 (2012) 455703.

[42] K.M.F. Shahil, M.Z. Hossain, V. Goyal, A.A. Balandin, Micro-Raman spectroscopy of mechanically exfoliated few-quintuple layers of Bi_2Te_3, Bi_2Se_3, and Sb_2Te_3 materials, Journal of Applied Physics, 111 (2012) 054305.

[43] P. Srivastava, P. Kumar, K. Singh, Crystal Symmetry Breaking in Few Quintuple Bi_2Te_3 Nanosheets: Applications in Nanometrology of Topological Insulators and Low-Temperature Thermoelectrics, Journal of Nanoscience and Nanotechnology, 14 (2014) 5856-5863.

[44] J.X. Zhang, Q. Li, P.J. Niu, Q.X. Yang, B.M. Tan, X.H. Niu, B.H. Gao, Effect of annealing temperature on microstructure and thermoelectric properties of bismuth–

telluride multilayer thin films prepared by magnetron sputtering, Materials Research Innovations, 19 (2015) S10-408-S410-412.

[45] S. Biswas, R. Bhattacharya, Two Valence Subbands in Single Crystals of Bismuth Telluride Doped with Lead and Its Electrical Properties, physica status solidi (b), 151 (1989) 193-201.

[46] I.G. Austin, The Optical Properties of Bismuth Telluride, Proceedings of the Physical Society, 72 (1958) 545.

[47] S.K. Mishra, S. Satpathy, O. Jepsen, Electronic structure and thermoelectric properties of bismuth telluride and bismuth selenide, Journal of Physics: Condensed Matter, 9 (1997) 461.

[48] E.H. Kaddouri, T. Maurice, X. Gratens, S. Charar, S. Benet, A. Mefleh, J.C. Tedenac, B. Liautard, Optical Properties of Bismuth Telluride Thin Films, $Bi_2Te_3/Si(100)$ and $Bi_2Te_3/SiO_2/Si(100)$, physica status solidi (a), 176 (1999) 1071-1076.

[49] S.D. Mahanti, P.M. Larson, D. Bilc, H. Li, Electronic Structure of Complex Bismuth Chalcogenide Systems, in: M.G. Kanatzidis, S.D. Mahanti, T.P. Hogan (Eds.) Chemistry, Physics, and Materials Science of Thermoelectric Materials: Beyond Bismuth Telluride, Springer US, Boston, MA, 2003, pp. 227-247.

[50] X. Wang, H. He, N. Wang, L. Miao, Effects of annealing temperature on thermoelectric properties of Bi_2Te_3 films prepared by co-sputtering, Applied Surface Science, 276 (2013) 539-542.

[51] A.A. Nadir, M.A. Nadir, V.A. Xayala, G. Samir Sh, G.K. Taira, M.M. Konul, A.N. Sergey, N.Z. Vladimir, Metal–Insulator Transition Induced by Temperature in $Bi_2Te_{3-x}Cl_x$ Layered Compound, Japanese Journal of Applied Physics, 50 (2011) 05FD04.

[52] J.C. Slater, Barrier Theory of the Photoconductivity of Lead Sulfide, Physical Review, 103 (1956) 1631-1644.

[53] Z. Zeng, P. Yang, Z. Hu, Temperature and size effects on electrical properties and thermoelectric power of Bismuth Telluride thin films deposited by co-sputtering, Applied Surface Science, 268 (2013) 472-476.

[54] H. Huang, W.-l. Luan, S.-t. Tu, Influence of annealing on thermoelectric properties of bismuth telluride films grown via radio frequency magnetron sputtering, Thin Solid Films, 517 (2009) 3731-3734.

[55] D.-H. Kim, G.-H. Lee, Effect of rapid thermal annealing on thermoelectric properties of bismuth telluride films grown by co-sputtering, Materials Science and Engineering: B, 131 (2006) 106-110.

[56] Y. Deng, H.-m. Liang, Y. Wang, Z.-w. Zhang, M. Tan, J.-l. Cui, Growth and transport properties of oriented bismuth telluride films, Journal of Alloys and Compounds, 509 (2011) 5683-5687.

[57] M.M. Rashid, K.H. Cho, G.-S. Chung, Rapid thermal annealing effects on the microstructure and the thermoelectric properties of electrodeposited Bi_2Te_3 film, Applied Surface Science, 279 (2013) 23-30.

[58] K. Kusagaya, H. Hagino, S. Tanaka, K. Miyazaki, M. Takashiri, Structural and Thermoelectric Properties of Nanocrystalline Bismuth Telluride Thin Films Under Compressive and Tensile Strain, Journal of Electronic Materials, 44 (2015) 1632-1636.

[59] Z.-k. Cai, P. Fan, Z.-h. Zheng, P.-j. Liu, T.-b. Chen, X.-m. Cai, J.-t. Luo, G.-x. Liang, D.-p. Zhang, Thermoelectric properties and micro-structure characteristics of annealed N-type bismuth telluride thin film, Applied Surface Science, 280 (2013) 225-228.

[60] Y. Zhou, L. Li, Q. Tan, J.-F. Li, Thermoelectric properties of Pb-doped bismuth telluride thin films deposited by magnetron sputtering, Journal of Alloys and Compounds, 590 (2014) 362-367.

[61] O. Vigil-Galán, F. Cruz-Gandarilla, J. Fandiño, F. Roy, J. Sastré-Hernández, G. Contreras-Puente, Physical properties of Bi_2Te_3 and Sb_2Te_3 films deposited by close space vapor transport, Semiconductor Science and Technology, 24 (2009) 025025.

[62] L.M. Goncalves, C. Couto, P. Alpuim, A.G. Rolo, F. Völklein, J.H. Correia, Optimization of thermoelectric properties on Bi_2Te_3 thin films deposited by thermal co-evaporation, Thin Solid Films, 518 (2010) 2816-2821.

[63] F. Cruz-Gandarilla, O. Vigil-Galán, J.G. Cabañas-Moreno, J. Sastré-Hernández, F. Roy, Structural and microstructural characterization of Bi_2Te_3 films deposited by the close space vapor transport method using scanning electron microscopy and X-ray diffraction techniques, Thin Solid Films, 520 (2012) 3865-3870.

Figures:

Fig. 1: Schematic of the e-beam evaporation system used to coat bismuth telluride thin films. The substrate holder shows four positions (numbered 1 to 4) separated by 3 cm.
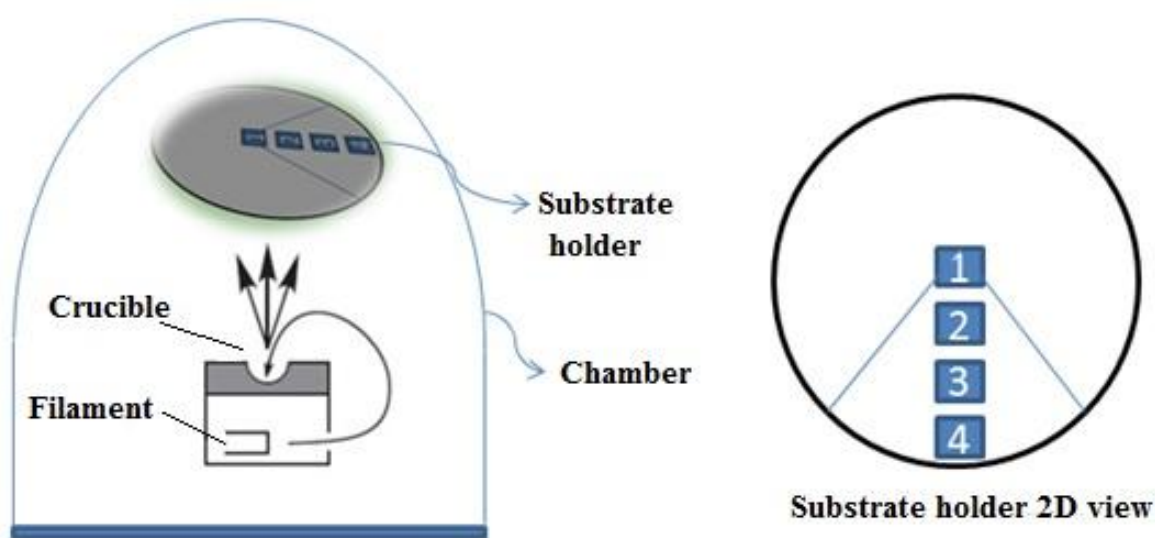
Fig. 2: (a) X-ray diffraction patterns of as-deposited (BT-AD) and annealed Bi_2Te_3 films (BT-T) along with the Rietveld refinement are given. Black symbols and red lines in the plot correspond to the measured intensities and calculated pattern. '*' in the patterns indicate impurity phase. (b) Lattice parameters (*a and c*), *c/a* ratio of as-deposited and annealed Bi_2Te_3 films are shown as a function of annealing temperature.
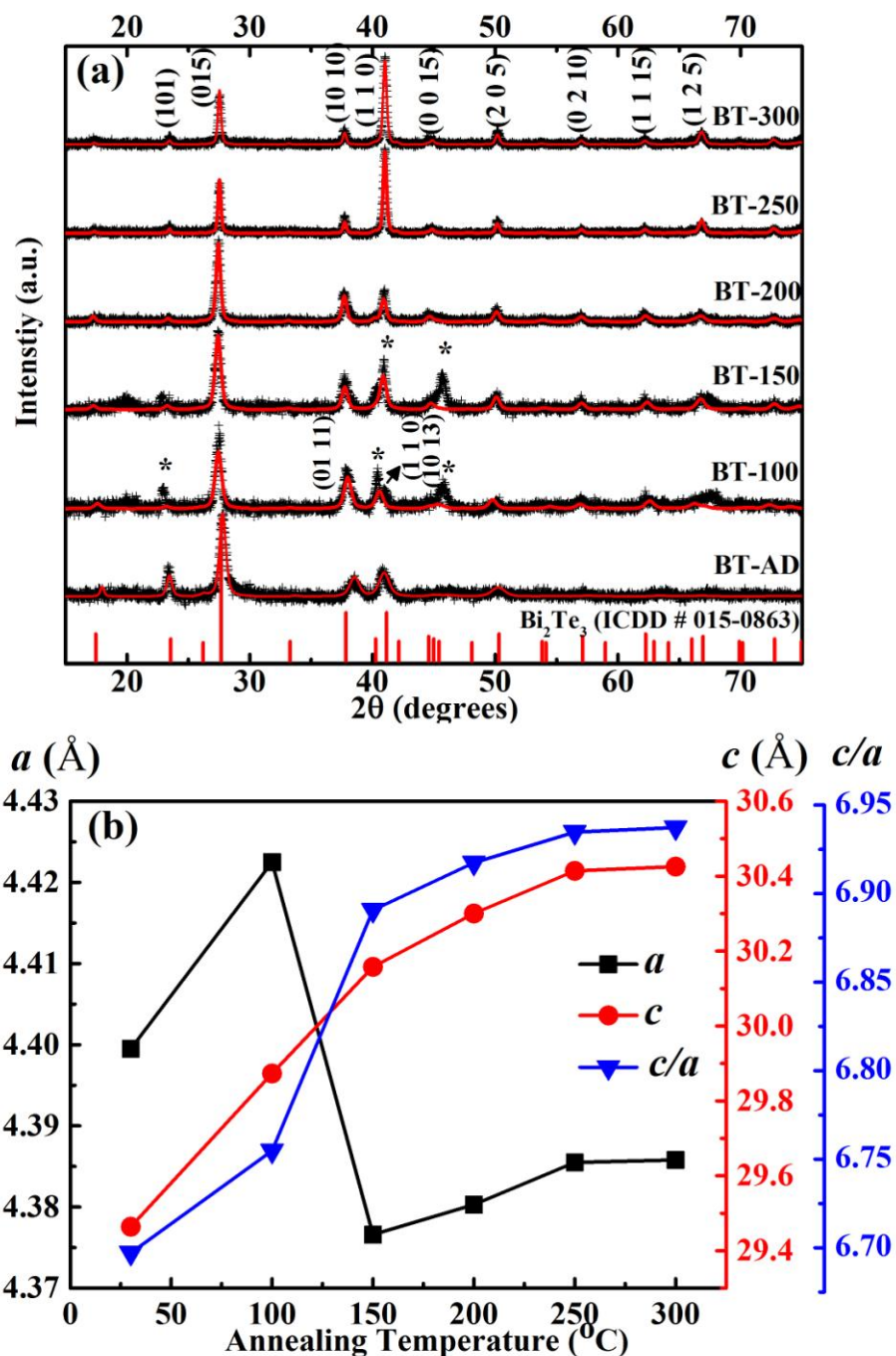
Fig. 3: Raman spectra acquired with an excitation laser source of wavelength 488 nmfrom the as-deposited and annealed Bi_2Te_3films. (a) The spectra in the range of 75 cm^{-1} to 1050 $cm^{-1}$is shown. (b) The magnified portion of spectra in the region between 75 cm^{-1} to 175 cm^{-1} showing the E_g^2, A_{1u} and A_{1g}^2 modes is given. (c) Shows the Raman spectral positions of the E_g^2, A_{1u} and A_{1g}^2 modes as a function of annealing temperature.
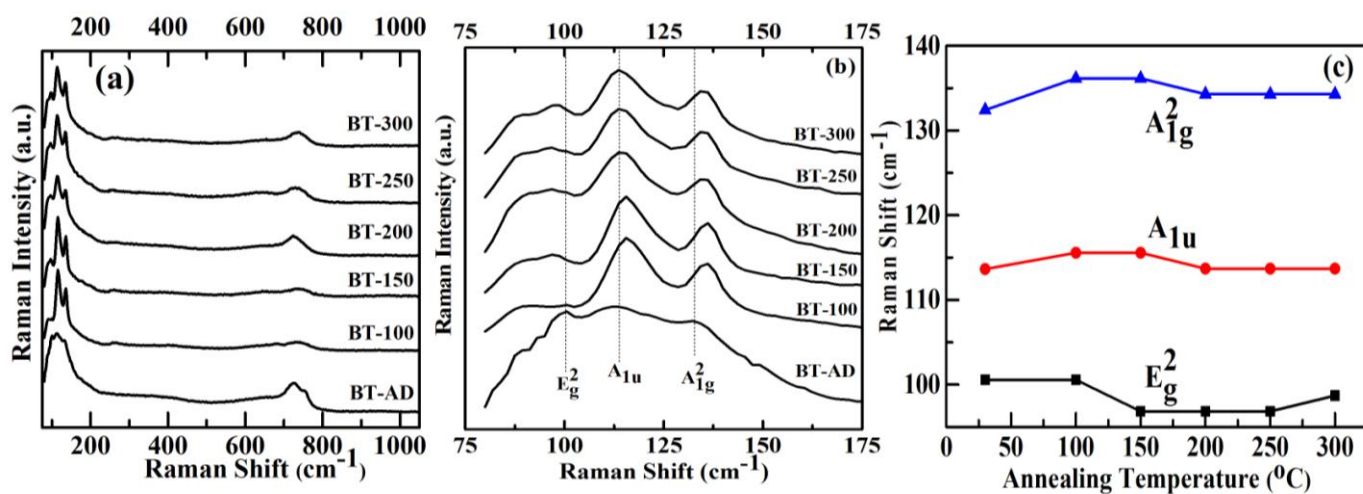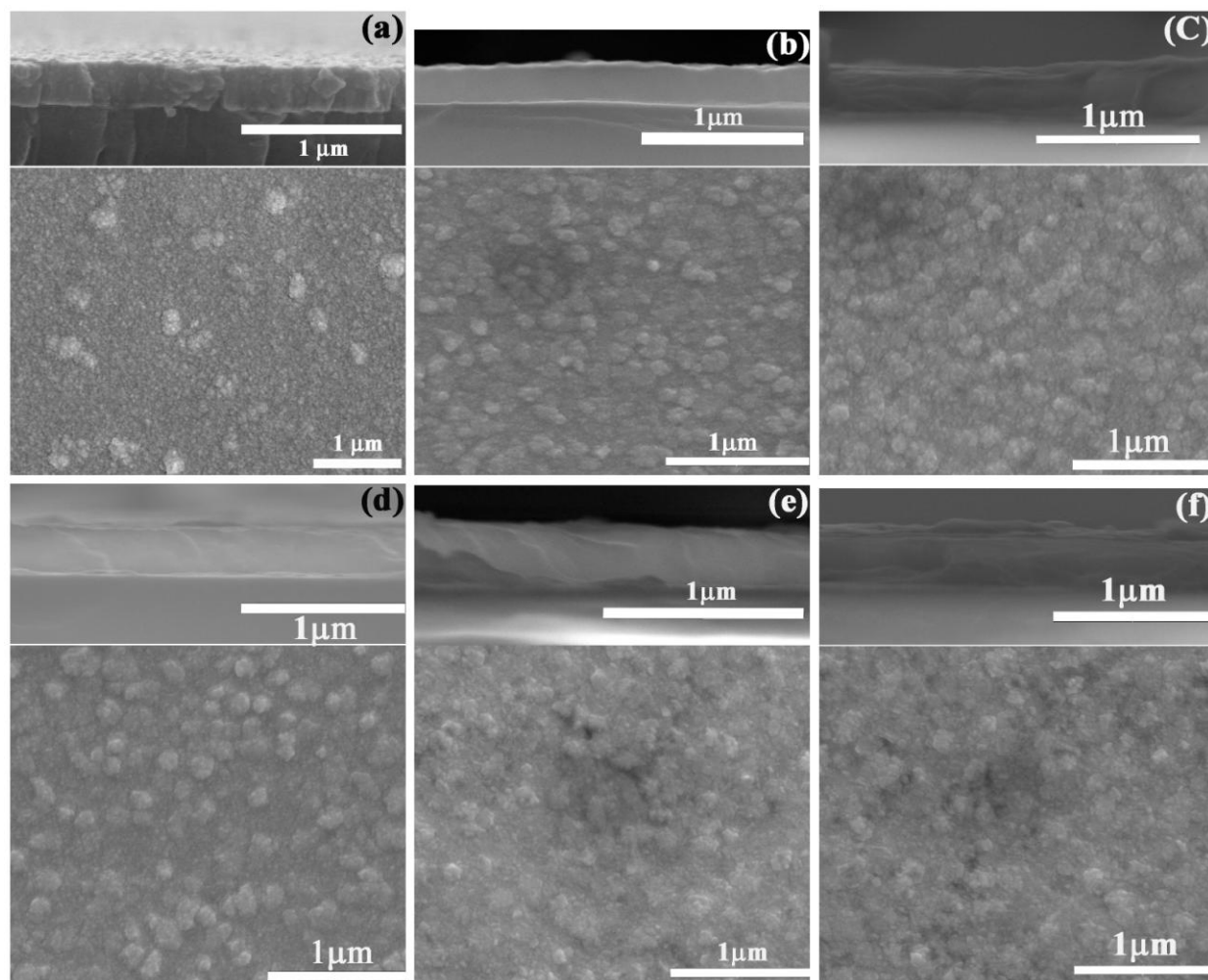
Fig. 4: FESEM images of as-deposited and annealedBi$_2$Te$_3$ films.(a) BT-AD, (b) BT-100, (c) BT-150, (d) BT-200,(e) BT-250 and (f) BT-300. Top and the bottom panels in each figure correspond to the cross sectional and topographic images of Bi$_2$Te$_3$ thin films.

Fig. 5: Atomic force microscopy images of as-deposited and annealed Bi_2Te_3 films. All the images correspond to 2 μm × 2 μm scan area. (a) BT-AD, (b) BT-100, (c) BT-150, (d) BT-200,(e) BT-250 and (f) BT-300.
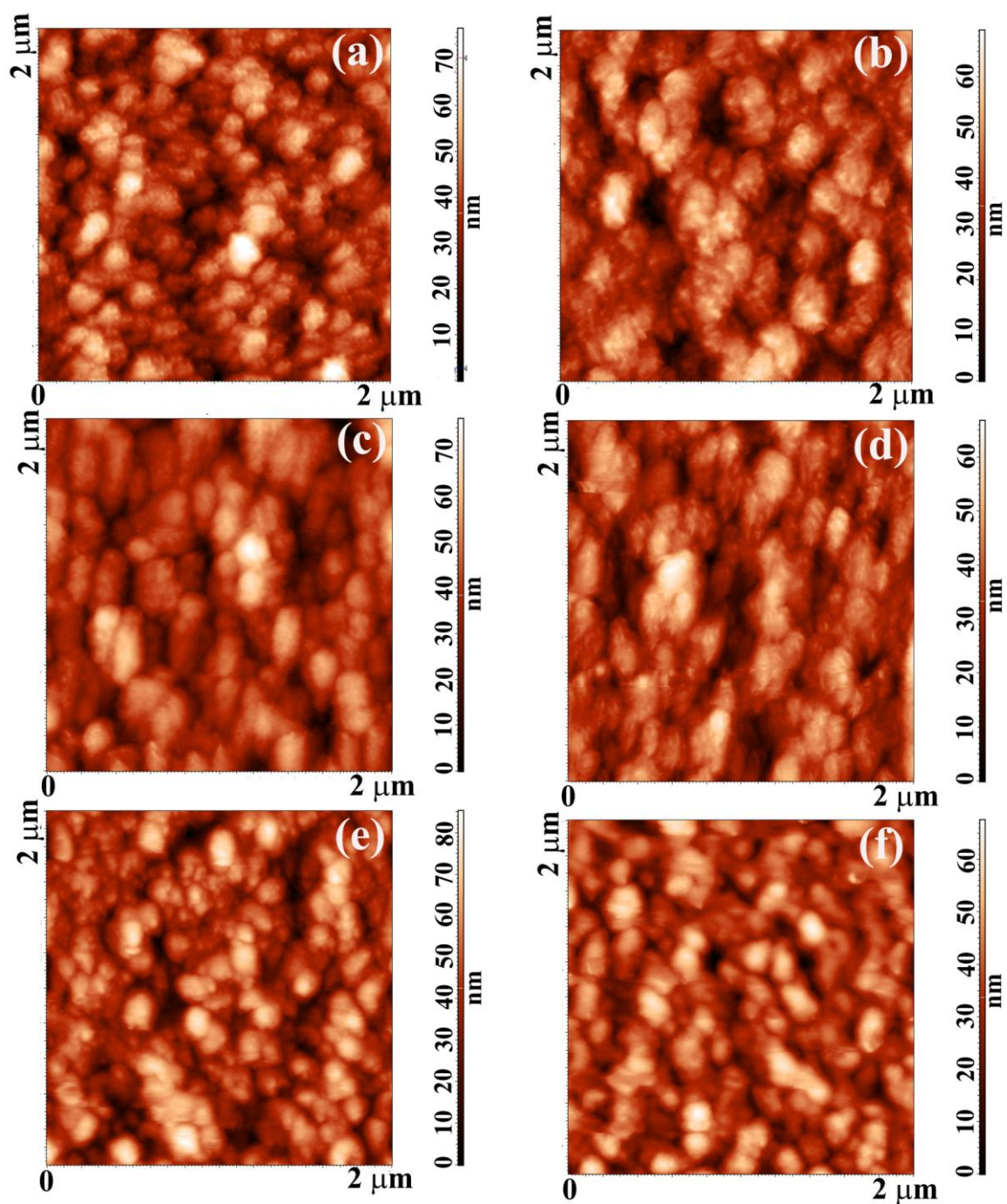
Fig. 6: Bright field transmission electron microscopy images (top panels) and corresponding SAED patterns (bottom panels) of Bi_2Te_3 films. (a) BT-AD, (b) BT-100, (c) BT-150, (d) BT-200, (e) BT-250 and (f) BT-300.
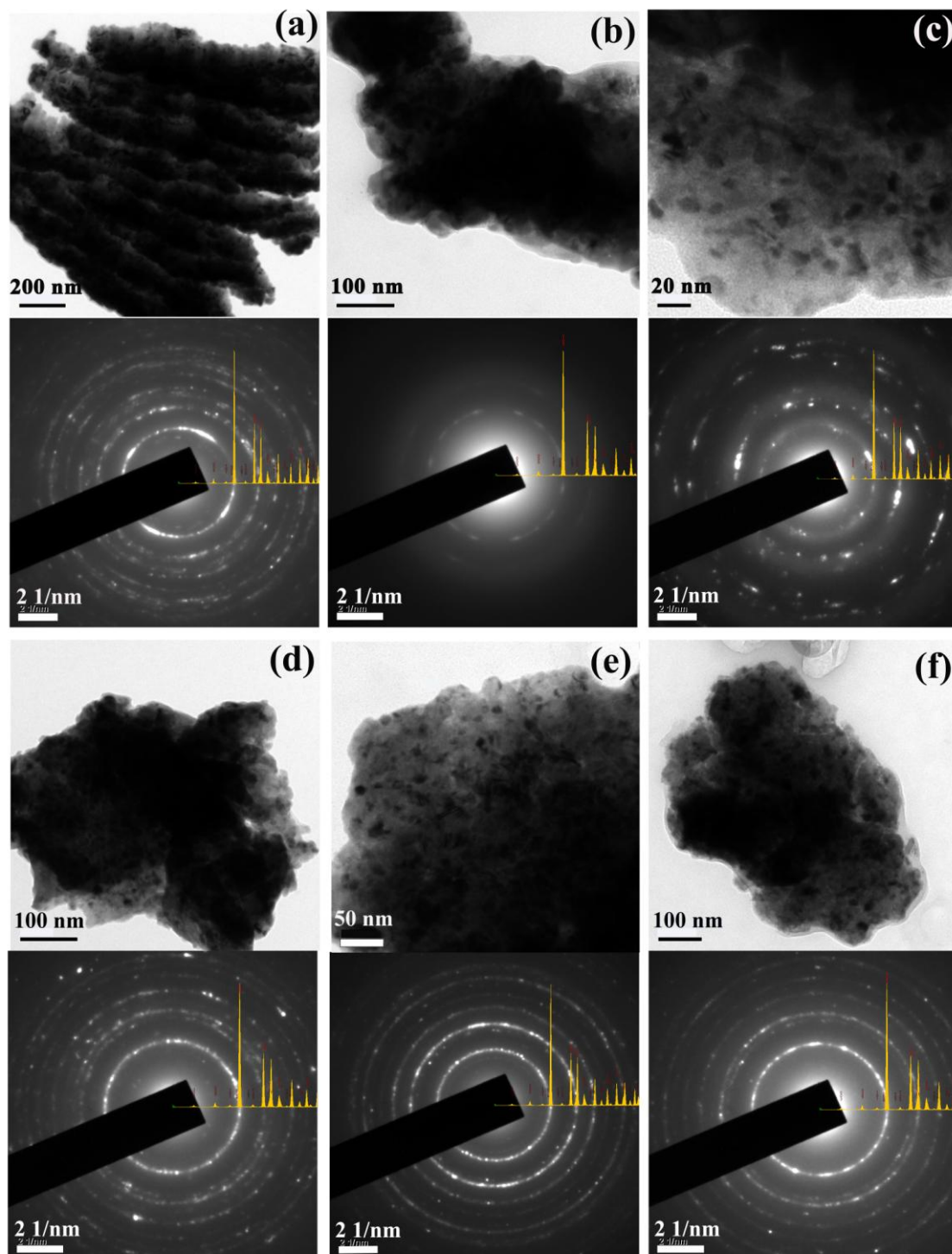
Fig. 7: High resolution transmission electron microscopy images of Bi$_2$Te$_3$ films. (a) BT-AD, (b) BT-100, (c) BT-150, (d) BT-200,(e) BT-250 and (f) BT-300.The arrow show regions where lattice images are distorted.
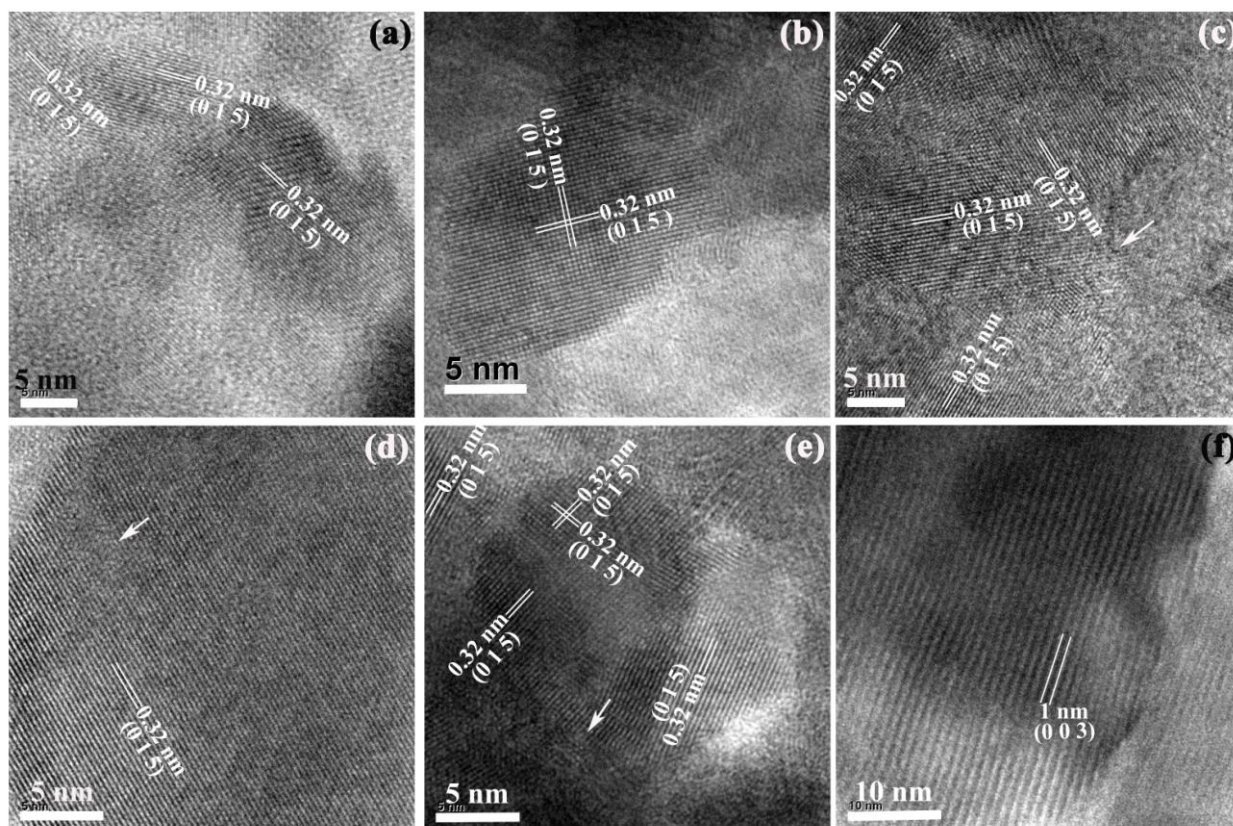
Fig. 8: (a) Diffuse reflectance spectra of BT-AD and BT-T Bi$_2$Te$_3$ films. (b) and (c) show the Kubelka-Munk transformed reflectance spectra of as-deposited and annealed Bi$_2$Te$_3$ films for a direct and indirect band, respectively.
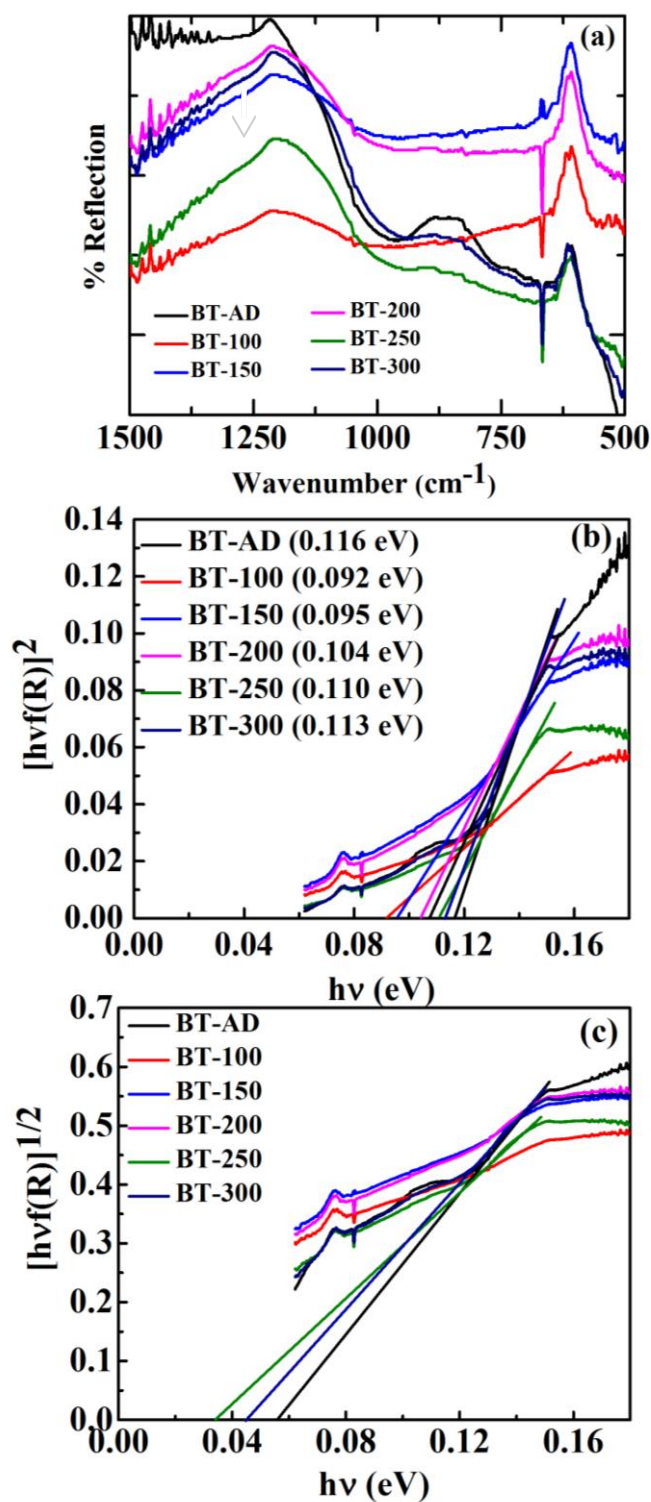
Fig. 9: Variation of carrier concentration and carrier mobility of BT-AD and BT-TBi$_2$Te$_3$ films measured at room temperature.
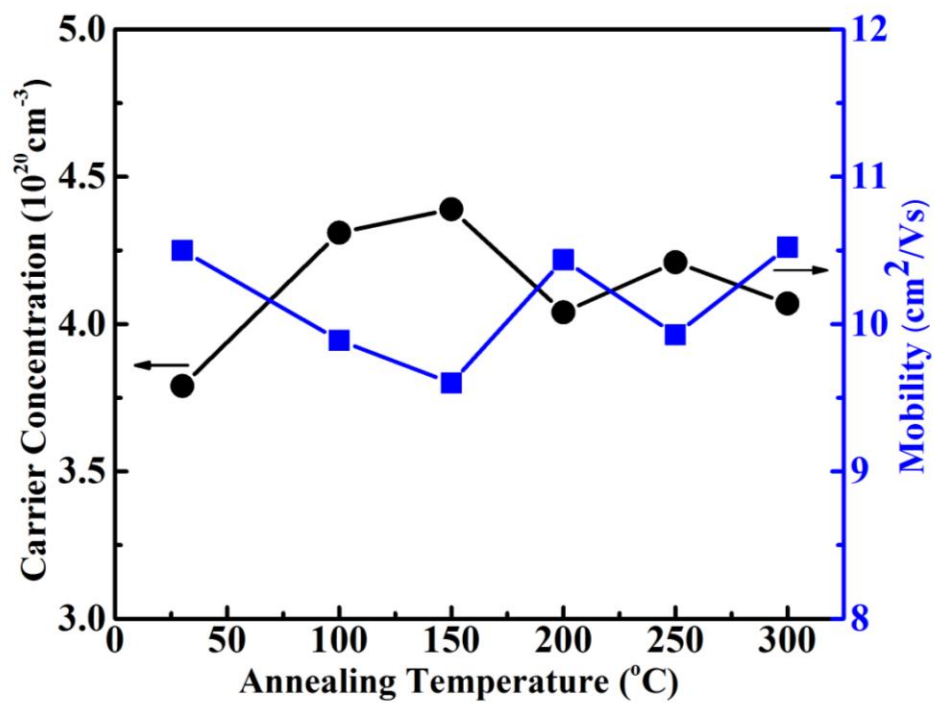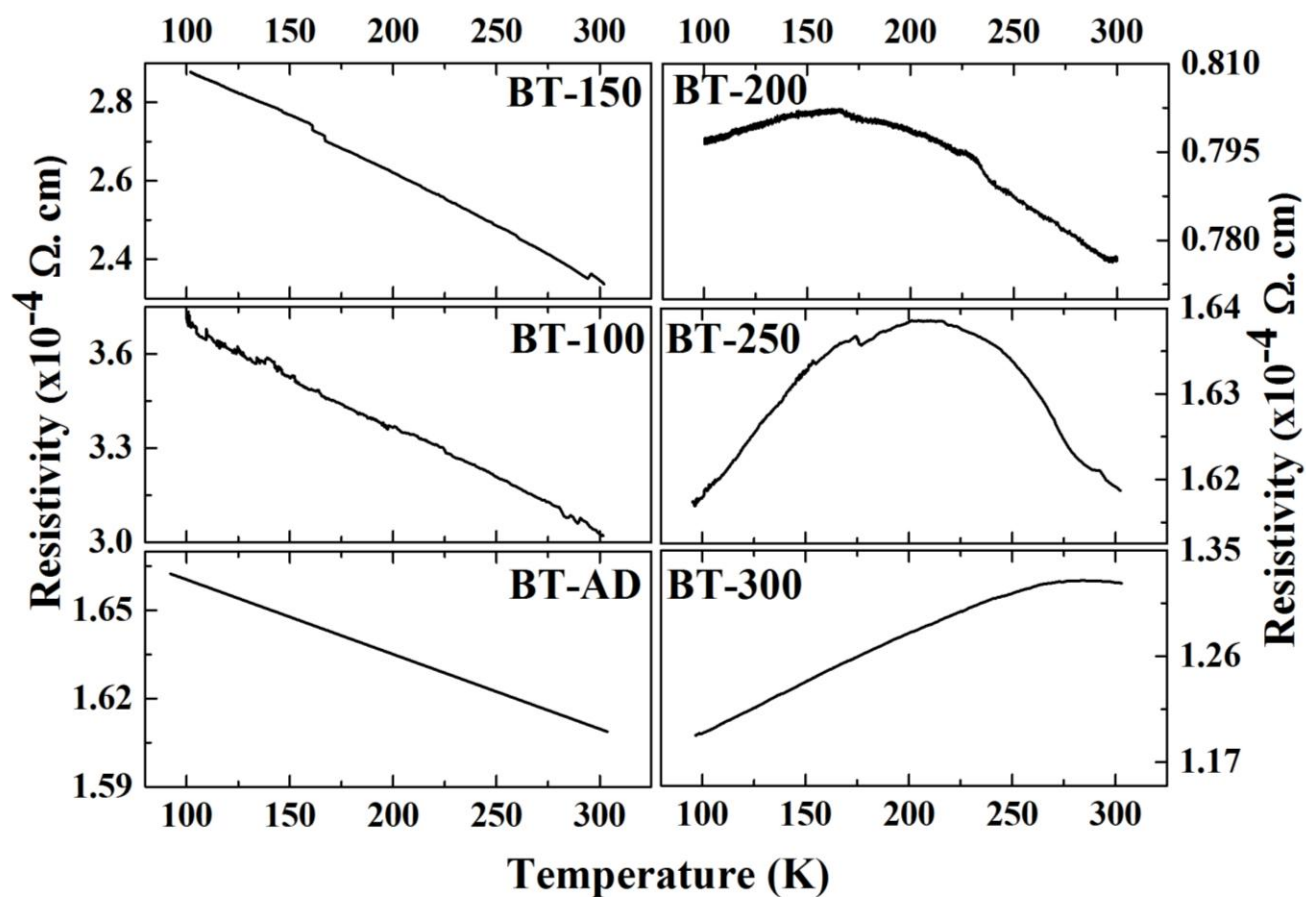
Fig. 10: Temperature dependence resistivity of BT-AD and BT-T Bi_2Te_3 films

Fig. 11: (a) Electrical and thermoelectric properties of BT-AD and BT-T Bi_2Te_3 films measured at room temperature. (b) The effect of applied temperature on power factor of BT-AD and BT-T Bi_2Te_3 films.
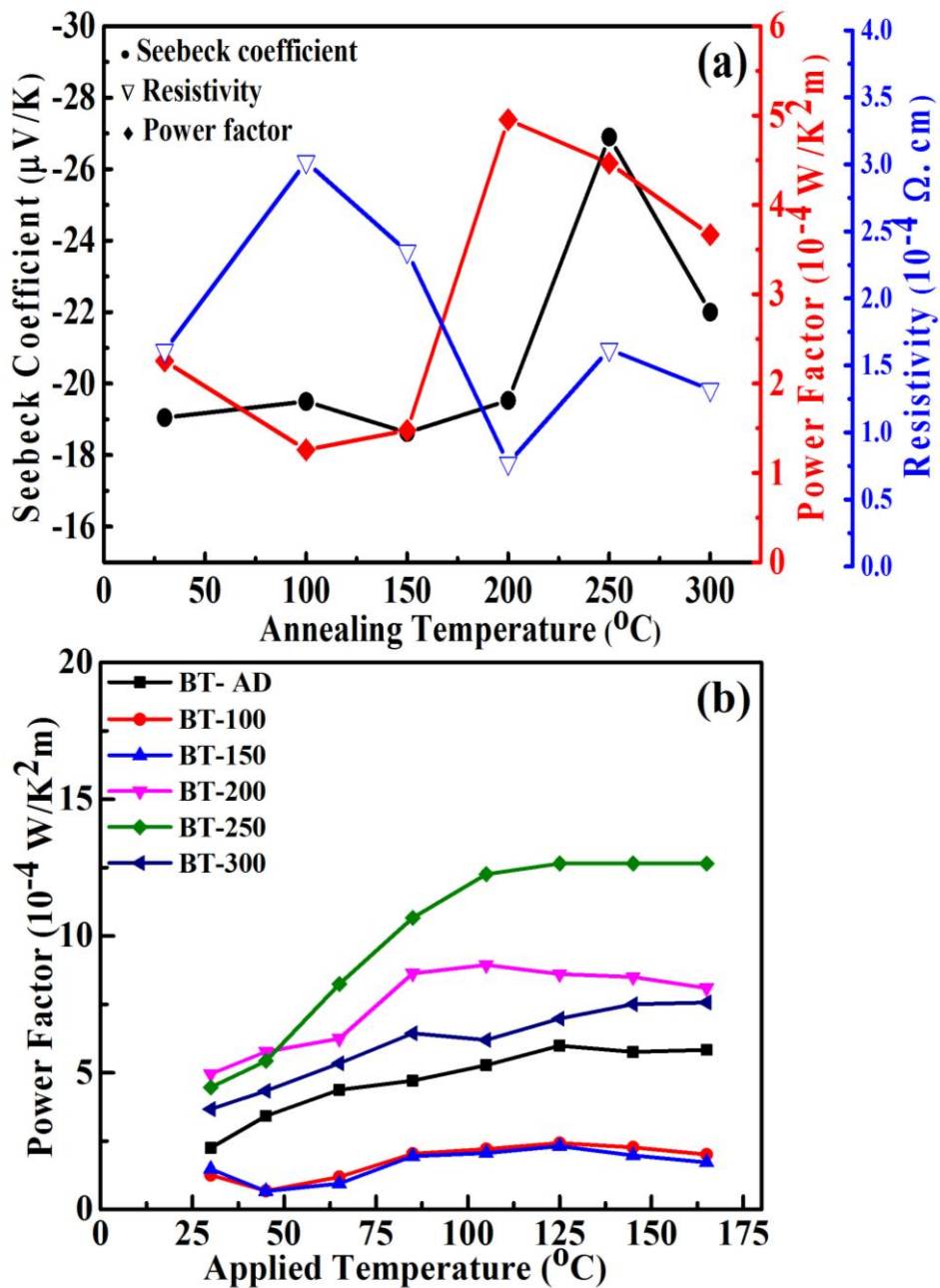
Table 1: The composition (Te:Bi ratio) of thin films deposited at various substrate positions (numbered 1 to 4 in Fig.1) and e-gun powers are tabulated. The elemental concentration is determined with an uncertainty of 0.5 *at.* %.

Position of the sample	45 watt Te:Bi (*at.* %)	67.5 watt Te:Bi (*at.* %)	90 watt Te:Bi (*at.* %)
1	51.4:48.6	61.7: 38.3	70.2:29.8
2	-	64.9: 35.1	-
3	-	70.1: 29.9	-
4	-	81.1: 18.9	-

Table 2: Structural lattice parameters, crystallite size and microstrain estimated from the Rietveld refinement of the x-ray diffraction patterns of Bi_2Te_3 thin films annealed for 60 min in vacuum (3×10^{-6} mbar). Estimated standard deviations are given in parentheses.

Bi_2Te_3 thin film	Crystallite size ($d \pm 10$ Å)	Micro strain (%)	Lattice parameter		
			a (Å)	c (Å)	c/a
BT-AD	133	0.075	4.3995(3)	29.4640(3)	6.697
BT-100	144	0.072	4.4225(3)	29.8732(2)	6.755
BT-150	165	0.071	4.3766(2)	30.1579(2)	6.891
BT-200	220	0.003	4.3803(1)	30.3003(9)	6.917
BT-250	332	0.016	4.3855(6)	30.4141(9)	6.935
BT-300	288	0.018	4.3858(2)	30.4255(6)	6.937

Table 3: Raman peaks in Bi_2Te_3 thin films

Bi_2Te_3	E_g^2 (cm^{-1})	A_{1u} (cm^{-1})	A_{1g}^2 (cm^{-1})	$I(A_{1g}^2)/I(E_g^2)$	$I(A_{1u})/I(E_g^2)$

thin film					
BT-AD	100.58	113.69	132.41	0.95	1.02
BT-100	100.58	115.56	136.15	1.64	2.04
BT-150	96.84	115.56	136.15	1.37	1.69
BT-200	96.84	113.69	134.28	1.07	1.24
BT-250	96.84	113.69	134.28	1.14	1.33
BT-300	98.71	113.69	134.28	1.13	1.33

Table 4: Composition form EDS, thickness from cross-sectional SEM, roughness from AFM and bandgap estimation from DRS studies of as deposited and annealed Bi_2Te_3 thin films

Bi_2Te_3 thin film	*at.* % (± 0.5 %)		Thickness (± 5 nm)	Average Roughness (± 0.1 nm)	RMS (± 0.1 nm)	Direct Bandgap (± 0.004 eV)	Indirect Bandgap (± 0.004 eV)
	Te	Bi					
BT-AD	61.7	38.3	288	8.3	10.5	0.116	0.034
BT-100	68.9	31.1	276	8.5	10.7	0.092	-
BT-150	64.3	35.7	273	8.5	10.6	0.095	0.044
BT-200	63.1	36.9	294	7.6	9.6	0.104	-
BT-250	61.4	38.6	293	10.8	13.4	0.110	0.056
BT-300	60.9	39.1	295	7.9	9.8	0.113	-

Highlights:

- Nanocrystalline Bi_2Te_3 thin films are fabricated by e-beam evaporation at 300 K
- Vacuum annealing lead to breaking of quintuple layer with (110) oriented crystallites
- Rearrangement of crystallographic planes leads to Te rich crystallite surface
- Bi_2Te_3 films gradually change from NTC to PTC behaviour on vacuum annealing
- Vacuum annealed Bi_2Te_3 thin films are favourable for thermoelectric applications